The Folded Pneumatic Artificial Muscle (foldPAM): Towards Programmability and Control via End Geometry

Sicheng Wang[1], Eugenio Frias Miranda[1], and Laura H. Blumenschein[1]

***Abstract*— Soft pneumatic actuators have seen applications in many soft robotic systems, and their pressure-driven nature presents unique challenges and opportunities for controlling their motion. In this work, we present a new concept: designing and controlling pneumatic actuators via end geometry. We demonstrate a novel actuator class, named the folded Pneumatic Artificial Muscle (foldPAM), which features a thin-filmed air pouch that is symmetrically folded on each side. Varying the folded portion of the actuator changes the end constraints and, hence, the force-strain relationships. We investigated this change experimentally by measuring the force-strain relationship of individual foldPAM units with various lengths and amounts of folding. In addition to static-geometry units, an actuated foldPAM device was designed to produce continuous, on-demand adjustment of the end geometry, enabling closed-loop position control while maintaining constant pressure. Experiments with the device indicate that geometry control allows access to different areas on the force-strain plane and that closed-loop geometry control can achieve errors within 0.5% of the actuation range.**

I. Introduction

The design and use of pneumatic artificial muscles (PAMs) remains an active field of research despite an origin that dates back to the early days of robotics [1]. This type of actuator is among the most common for soft robots [2], and has also been used in a wide range of applications such as in haptic devices [3] and prosthetics [4]. Typically, a PAM has only a single degree of freedom but that degree of freedom can produce contraction, expansion, bending, and more upon application or removal of air pressure [5], [6], [7].

Existing PAM designs can be classified based on their material and principle of motion. Here, we simply classify them into the categories of "elastomer-based" and "thin-filmed" actuators. The elastomer-based PAM designs feature partially constrained flexible material that expand or contract elastically upon change in pressure. McKibben Pneumatic Muscle [1] and the Pleated Pneumatic Artificial Muscle [8] are such type of actuators that have a single air bladder and flexible, enveloping constraints. The fabric PAM [9] further develops the concept by synthesizing the functions of the bladder and the constraint into a single chamber made of highly compliant, air-tight, bias-cut fabric. The PneuNet actuator [10], in contrast, has network of multiple interconnected, elastic air chambers with constraint by material thickness or embedded fibers.

Thin-filmed PAMs, on the other hand, feature a thin, nearly inelastic but flexible film fabricated into a pouch. Examples within this class of actuators are often relatively simple to manufacture, involving procedures such as heat stamping, as for Peano/AeroMorph actuators [11], or attaching rigid diametric constraints on a thin-film tubing segment, as in Serial Pneumatic Artificial Muscles (sPAM) [12] and Bubble Artificial Muscles (BAM) [13]. Both linear and rotational motions may be achieved and the concept has also inspired the design of actuators based on other forms of energy and materials, such as the HASEL-Peano actuator [14].

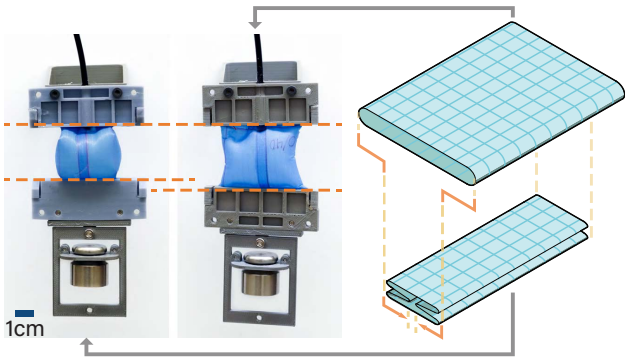

Fig. 1. The conceptual illustration of the foldPAM, showing its cross-section and different strains produced by foldPAM units with a fold ratio (f_r) of 0.4 (left) and 0 (right) respectively, when subjected to a load of approximately 50g mass.

For most of the PAM designs, the force and displacement produced by an actuator at a given input pressure is a functional relationship determined by its physical construction. With emerging applications that demand precise control over both force and displacement, the programmability of PAMs has received increased attention. Methods to design and fabricate actuators to match desired trajectories and ranges of motion have been developed, especially for elastomer-based actuators as its structure enables a large design space with many parameters: actuators capable of producing a range of curvatures and torsions can be programmed by varying the orientation of constraining fibers and material stiffness [15], selectively applying elastic and inelastic fabrics as constraint on a McKibben-type actuator [16], and varying the relative position of air channels connecting consecutive air chambers of a PneuNet actuator [17]. A mechanism for actively modifying the behavior of an actuator by varying enclosure fiber angle was developed by Yoshida et al. [18].

For the thin-filmed PAMs, the programmability at a single-unit scale can be achieved by varying the geometry, for example the dimension of a heat-sealed pattern at the middle of a Pouch Motor [11]. While a number of geometric parameters have been shown to affect the behavior of the

[1]School of Mechanical Engineering, Purdue University, IN 47906
*Email: {wang5239, efrias, lhblumen}@purdue.edu

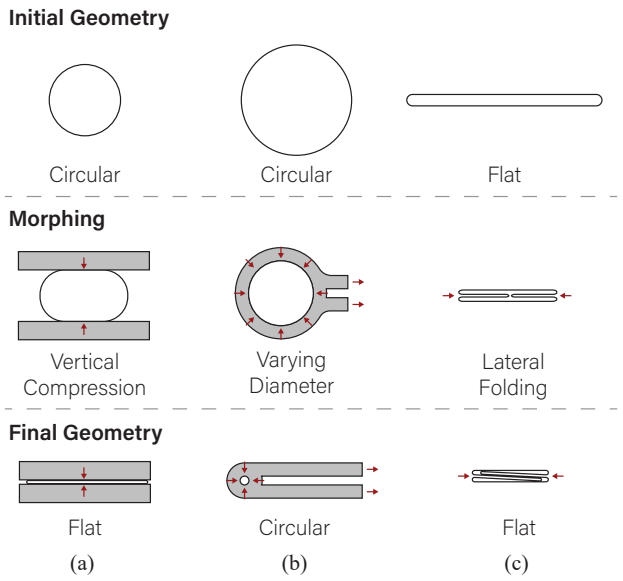

Fig. 2. Three examples of parameterized end geometry. (a): initially a circular section of the inflated tube, each end of the actuator is compressed till its vertical height is zero; (b) initially a circular section with the same diameter as the tube, its diameter shrinks under an external constriction to attain a near-zero diameter; (c): initially flattened at each end, a pair of symmetric, lateral folds are created at both edges of the actuator, whose total width varies from zero to $2/3$ of the initial actuator width.

thin-filmed PAMs, for example the aspect ratio [19] and end radius [13], such effect is more often considered from an optimization point of view, where maximizing metrics such as zero-tension strain and maximum force output is the primary concern.

In this paper, we propose a new concept for programmable thin-filmed PAM, the folded Pneumatic Artificial Muscle (foldPAM), constructed by a short segment of inextensible thin-film tubing that is folded symmetrically with respect to its principal axis. Adjusting the amount of folding results in a tunable force-strain relationship, allowing behaviors ranging from Pouch Motor like [20] to a limit of sPAM like [12]. The force-strain relationship can be pre-configured or adjusted on-demand when an additional actuated degree of freedom is added. Actuating the folding further enables regulating the foldPAM output while at a constant input pressure.

In the following sections, we first discuss the notion of altering the actuator behavior by changing its end geometry. We then describe the design and fabrication of the foldPAM with static geometry, followed by experimental results for the force-strain curves produced by a foldPAM, compared to existing modeling results, with various design parameters. This experimentation produces a "design space" as a collection of all possible force-strain curves. We then present the design and characterization of a foldPAM with active, reconfigurable geometry ("Active foldPAM"). Finally, we demonstrate the Active foldPAM controlling its output position under a step-change in external load using end geometry.

II. Design and Control via End Geometry

As noted in several previous studies such as [12] and [13], the inflated geometry, and hence the force-displacement relationship of a serial Pneumatic Artificial Muscle (sPAM) or Bubble Artificial Muscle (BAM) is affected by the diameter of the constriction at the ends. Drawing inspiration from these results, we may then hypothesize that for other thin-filmed actuators the force-strain relationship may also be modified by manipulating the end constraints – in other words, we can utilize end geometry to pre-program or control in real-time the behavior of an actuator.

To implement this strategy, we need to find a parameterizable geometry such that a range of actuator performance can be obtained by varying one or more geometric parameters. Figure 2 gives several examples of potential end geometry variations for actuator control, where the displayed shape describes the cross section of a inflated, thin-film chamber that is readily compressible. In Figure 2(a) the chamber section varies from the original circular shape to one that is fully compressed flat. Without any compression, the "actuator" would have zero force and displacement; at full compression it takes the form of a pouch motor [20], and a spectrum of actuators is obtained from the intermediate states. Likewise, as the section in Figure 2(b) is compressed to a minimal area by a variable-diameter, circular constraint, the actuator evolves from a plain piece of tubing to a sPAM unit.

The folded geometry shown in Figure 2(c) is the geometry of interest for this work. In this concept we begin with a fully compressed end section, such that the actuator has the behavior of a pouch motor [12]. We then introduce a pair of symmetric folds with respect to the center of the actuator. As increasing amount of material is folded in the actuator, the width of the actuator reduces; at maximum folding, the width of the actuator reduces to 33.3% of its original width, and the folds of the two sides fully overlap.

In the following sections, we use the folded end geometry to illustrate two ways to utilize the concept: (a) the "static geometry" actuator, by fabricating actuator units in certain end-geometry parameters to pre-program a desired force-displacement profile; (b) the "active geometry" actuator, by designing actuators with mechanisms that actively changes the end geometry to produce force-displacement profiles that match a variety of working conditions.

III. Static Geometry foldPAM

A. Design and Fabrication

In describing the design and fabrication process of a static foldPAM unit, we first introduce the parameters used to define a foldPAM actuator in general. The relevant variables and directions are illustrated in Figure 3(a). The actuator is made of a section of thin film tubing flattened to a rectangular piece of length l_0 and width $W_0 = \pi D_0/2$, where D_0 is the inflated diameter of the tubing. Each of the edges along the axial direction is then folded laterally in between the surfaces of the tubing by a distance of $w_f/2$, where w_f is the total folded width on each side, resulting in an actuator with uninflated width of $W = W_0 - w_f$. As a result, the geometry of a foldPAM unit can be described by two normalized quantities, fold ratio f_r and aspect ratio a_r, defined by the

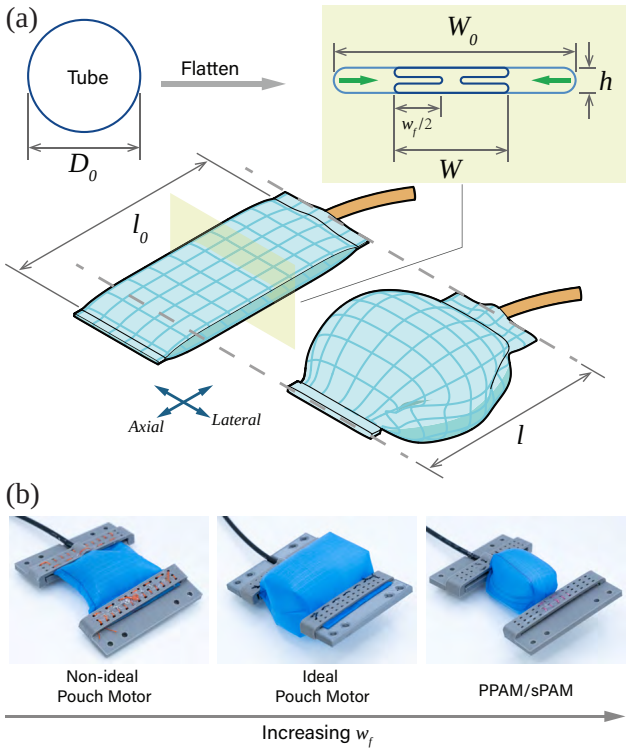

Fig. 3. (a): A conceptual illustration of the foldPAM, showing all relevant variables. (b): three stages that the foldPAM undergoes as its f_r increases from 0 to 0.67: non-ideal pouch motor, ideal pouch motor, and sPAM/PPAM.

following equations:

$$f_r = \frac{w_f}{W_0},\ a_r = \frac{l_0}{W_0}. \tag{1}$$

Finally, the folded tube is sealed at both ends, retaining the tubing in the folded state.

A foldPAM unit may be constructed with virtually any thin film that is flexible, near non-stretchable, and airtight. In this work we fabricated foldPAMs with 70μm thick, silicone-impregnated, rip-stop nylon fabric (Seattle Fabrics, WA) and the ends were sealed with a silicone adhesive (Sil-Poxy, Smooth-On Inc., PA). Figure 4 shows the fabrication process.

B. Workspace Prediction with Existing Actuator Concepts

For a given aspect ratio a_r, as the fold ratio f_r varies from 0 to 0.67, the foldPAM can be seen as morphing through three states that are similar to existing actuator designs. As shown in Figure 3(b), at $f_r = 0$, a foldPAM behaves like a non-ideal pouch motor [20] with a length of l_0 and a width of W_0, since it is subjected to a loss of maximum force and strain due to its finite width. Currently, there lacks an analytical model that describes such boundary effect, though works such as Veale et al. [19] have investigated the effect of pouch geometry experimentally. As w_f increases, the behavior of the actuator approaches an ideal pouch motor, as the folded portion provides additional material to compensate for the boundary effect. When the folded portion is sufficient to allow a circular section for the inflated actuator, i.e.,

$$w_{f,circ} = \frac{2l_0}{\pi}, \tag{2}$$

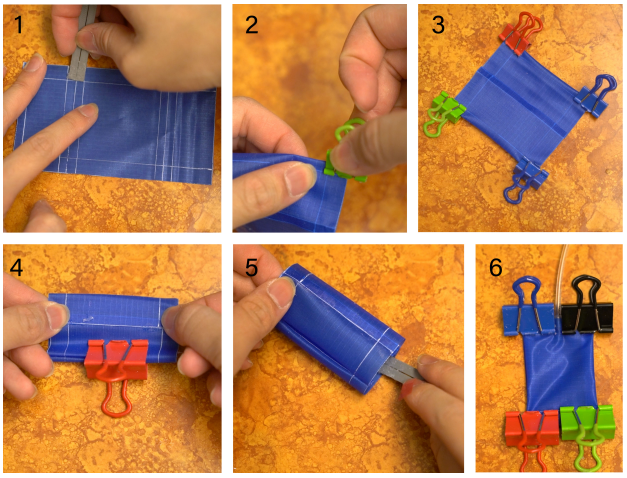

Fig. 4. Fabrication process of a static foldPAM unit. (1): Apply silicone adhesive to the ends of the folded portion; (2) and (3): use a clip to hold the folds until the adhesive cures; (4): Apply adhesive and form a hoop from the fabric piece with a lap joint along the axial direction; (5) Apply adhesive at the ends and insert a piece of thin tubing with double-sided tape (True Tape, LLC., CO) wrapped at one end (to allow bonding with the applied adhesive); and (6): use clips to hold the ends of the unit until the adhesive cures to ensure air-tightness.

the actuator becomes an ideal pouch motor, as in Figure 3(c). The force F and strain ε of the actuator, parameterized by $\theta \in (0, \frac{pi}{2}]$, is given in [20] by

$$F(\theta) = (W_0 - w_{f,circ}) l_0 P \frac{\cos\theta}{\theta} \tag{3}$$

$$\varepsilon(\theta) = 1 - \frac{\sin\theta}{\theta}, \tag{4}$$

where P is the pressure to which the actuator is inflated, and the strain ε for an actuator contracted to a length of l is defined as

$$\varepsilon = 1 - \frac{l}{l_0}. \tag{5}$$

When the actuator reaches the maximum f_r, as in Figure 3(d), we approximate its force-strain behavior by the serial/Pleated PAM (sPAM/PPAM) model [12]. We take the approximation because the actuator is highly constricted at the ends and has a large apparent aspect ratio (l_0/W) at high fold ratios, as similar to the two existing class of actuators. For a given contraction ε, the force produced by the maximally folded foldPAM is given by

$$F(\varepsilon) = \pi P h^2 \frac{1-2m}{2m\cos^2\phi}, \tag{6}$$

and m, ϕ are constants satisfying

$$\begin{aligned} \frac{E(\phi\backslash m)}{\sqrt{m}\cos\phi} &= \frac{l_0}{h}(1-\frac{\varepsilon}{2}) \\ \frac{F(\phi\backslash m)}{\sqrt{m}\cos\phi} &= \frac{l_0}{h}, \end{aligned} \tag{7}$$

where $F(\phi\backslash m)$ and $E(\phi\backslash m)$ are incomplete elliptic integral of first and second kind respectively, and we use the overall thickness of the actuator h, as indicated in Figure 3 to replace the term for end constriction radius in the sPAM/PPAM

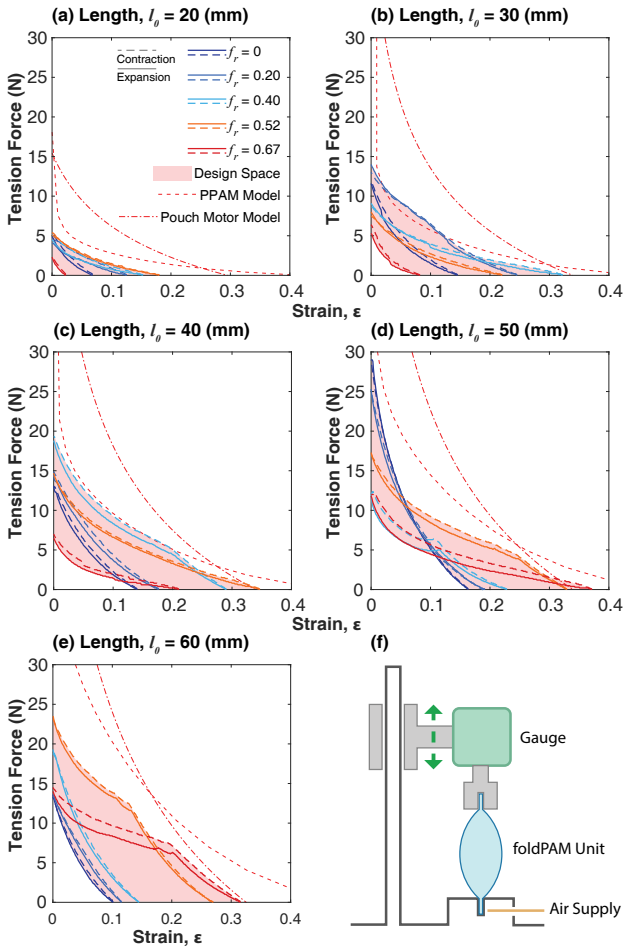

Fig. 5. (a)-(e): force-strain plot of static foldPAM units. All units have a constant W_0 of 50mm and l_0 varies from 20-60mm, resulting in a_r ranging from 0.4 to 1.2. The predictions by PPAM and Pouch Motor models are superposed with the data, and the design space bounded by the experimental force-strain curves is labeled by the shaded area. (f): Schematic of the testing apparatus for the experiment.

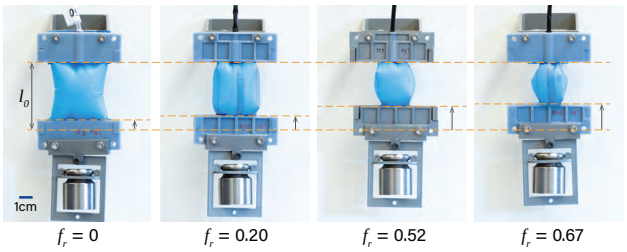

Fig. 6. A comparison of static-geometry foldPAMs with fold ratios f_r of 0, 0.20, 0.52, and 0.67. The units all have an initial length l_0 of 50mm, are inflated to a pressure of 12.4 kPa, and subjected to a load of 1N. Note that the amounts of strain observed here reflect their relative magnitude in Figure 5(d).

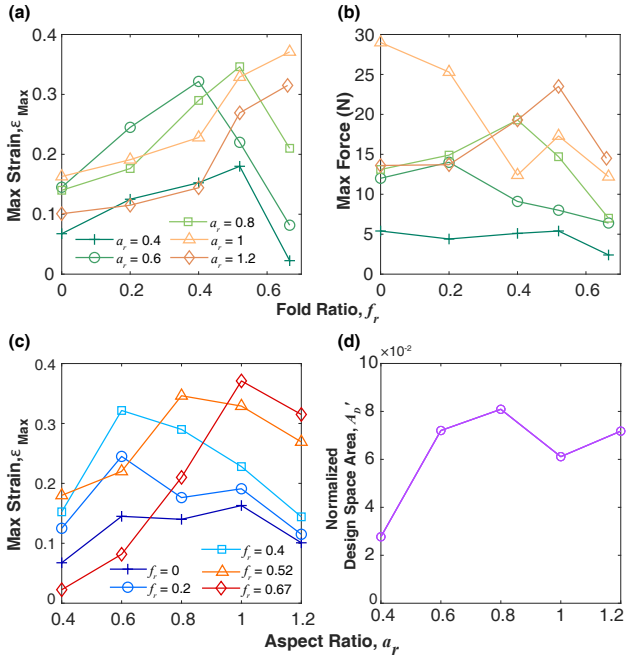

Fig. 7. (a) The maximum strain' of different l_0 over f_r's. It is desirable to use the shorter length foldPAMs for their linearity, while longer foldPAM lengths can reach higher strains. All units have a constant W_0 of 50mm and l_0 varies from 20 mm. (b) Maximum force of different l_0 over f_r's. Maximum force decreases as f_r increases. (c) The Maximum stress' of different l_o over five a_r's. From a_r 0.5 to 1, notice a flattening in f_r 0 to 0.4 while we observe a steep increase in contraction ratio and decreasing at higher f_r 0.52 and 0.67. (d) Area of Design Space and a_r relationship which is monotonic positive. As f_r increases, a higher max strain and lower force are observed.

model. In summary, while there is not an analytical model that describes the non-ideal pouch motor state, making it difficult to predict the no-folding limit of the foldPAM performance, We hypothesize that the pouch motor and sPAM/PPAM models predict the location of the force-strain curves when the foldPAM attains these states.

C. Experimental Methods

We tested a matrix of individual foldPAM units with different combinations of fold ratios and aspect ratios to obtain their force-strain relationships. The units were fabricated using the method described in Section III-A with aspect ratios $a_r \in [0.4, 1.2]$ with an incremental step of 0.2, and fold ratios $f_r = 0, 0.2, 0.4, 0.67$. The unfolded width W_0 is held constant at 50mm for all tested units, so the sequence of a_r thus gives initial lengths l_0 ranging from 20mm to 60mm. The testing units were sewn into a pair of custom-made, rigid fixtures and were mounted to a force gauge (Series 7, Mark-10 Corporation, NY) installed on a motorized travelling test stand (ESM 303, Mark-10 Corporation, NY). This setup is illustrated in Figure 5(f).

The force gauge had an initial position such that the distance between two ends of the testing unit was the maximum without inducing any tension in the uninflated foldPAM unit. After the foldPAM was pressurized to 12.4kPa, the force gauge then travelled at a constant rate of 15mm/min, gradually compressing the pressurized actuator to the zero-force, maximum contraction state, and then returning to the initial position. The force was recorded at a rate of 5Hz during the experiment, and the corresponding strain of the actuator was deduced from the known constant travel rate. The testing units pressure was regulated by a pressure control valve (QB3, Proportion Air, McCordsville, IN) for all tests.

D. Result and Discussion

1) Force-Strain Characteristics: The results of the force-strain experiment can be seen in Figure 5(a)-(e) broken down by length. We see that, in general, as f_r increases the max strain increases and the max force decreases. Additionally, for smaller fold ratios, i.e. f_r =0, 0.2, and 0.4, the max strain increases as l_0 or a_r increases. Figure 6 shows foldPAMs with $l_0 = 50$mm inflated to a pressure of 12.4kPa and subjected to a constant load of 1N, effectively showing a horizontal "slice" of the data. These trends can be further seen in Figure 7(a) and (b), which show the max strain and max force as a function of fold ratio, and Figure 7(c), which shows the max strain as a function of aspect ratio.

While these trends describe the majority of the data, we see some interesting behaviors at high aspect ratio and fold ratio. In several experiments with $f_r \geq 0.4$, we observe a "kink" in the force-strain curve, dividing the curve into two linear regions and giving a slower rate of increase in force output towards zero strain. This behavior indicates a sudden change in volume expansion during the eversion of the folded pouch, and fabricating the actuator with a more compliant material would likely reduce the extent of the behavior.

Examining the max strain as a function of aspect ratio (Figure 7(c)) we can see behavior similar to previous experimental measurements of pouch motors and sPAMs. For pouch motors, Greer et al. [12] experimentally demonstrated that at aspect ratios between 0.5 and 1 the maximum strain approaches the theoretical limit. We see similar behavior at lower fold ratios, seen in a flattening observed in f_r's 0, 0.2, and 0.4. For sPAMs, Greer et al. shows the strain increases with aspect ratio up to a peak near $a_r = 1.5$. We can observe the transition to sPAM-like behavior for fold ratios 0.52 and 0.67, with the maximum strain and the aspect ratio that sees the peaking of strain approaching, but remaining under, the values reported for sPAMs.

2) Relating to Model Prediction: We can additionally use the data to analyze the models presented in Section III-B. When these models are plotted against the data in Figure 5, we note that the sPAM/PPAM model generally predicts higher force and strain output, and the pouch motor model often predicts a higher force output but approaches the experimental results near the maximum strain. The deviation may indicate a loss of both force and strain due to material elasticity and the different geometry of the foldPAM during volume expansion. For pneumatic actuators the expected force is given by $dF = PdV$, where P is the internal pressure and dF, dV are differential changes in the force and volume of actuator. At higher strain where the actuator is nearly fully inflated, we see less volume loss and the ideal pouch motor model predicts the actuator behavior accurately for w_f near the value given in Equation (2), especially for greater actuator length and higher aspect ratio. However, at lower strain, the folded portion of the actuator reduces the volume of the actuator when not fully inflated, resulting in a lower force than the models predict. This effect is particularly pronounced at higher fold and aspect ratios. At maximum fold ratio, the folding limits the lateral expansion and results in a non-circular cross section, which deviates from the assumption by the sPAM/PPAM models, and the model approximates the measured data only for a limited number of cases. At low aspect ratios such as when $a_r \leq 0.8$, the apparent aspect ratio (l_0/W) of the actuator remains low even with a maximum fold ratio, making it more appropriate to consider the actuator as an under-inflated pouch motor than a sPAM/PPAM. Overall, while the pouch motor model partially predicts the force-strain relation at the ideal pouch motor model state, there lacks analytical models that predicts the behavior of the foldPAM near the other two states well without significant correction. Developing better insights to the behavior of foldPAM is a focus of the ongoing works.

3) Design Space Analysis: The results in Figure 5 for each length of the tested unit bound an area in the force-strain plane. As we expect continuously changing behavior when the parameter f_r is tuned, every combination of force and strain within the bounded area is reachable for some f_r at a given pressure. Thus, we define the bounded area as the "design space", A_D, representing the amount of reachable area on the force-strain plane for the foldPAM. Clearly, as A_D depends on the minimum and maximum force output, it would be a function of the internal pressure and the cross-section area of the actuator; and since it is difficult to measure the cross-section for different fold ratios, we define a normalized design space A'_D based on pressure and the unfolded area of the actuator, which correlates with the cross-section area, as follows:

$$A'_D = \frac{A_D}{a_r {W_0}^2 P}. \tag{8}$$

The value of A'_D obtained at each aspect ratio is shown in Figure 7(d). We see that except for $a_r = 0.4$ where both force and strain diminishes, A'_D fluctuates near a constant value of approximately 0.06. This indicates that the design space area is relatively independent of the aspect ratio of the actuator, and rather scales with pressure and dimension.

Overall, the experimental data suggest that the foldPAM behavior is similar to both pouch motor and sPAM behavior depending on aspect and fold ratio. The design space analysis suggest foldPAMs can be made for a wide range of force-strain curves, but additional modeling would be needed to a priori predict a foldPAM's behavior.

IV. Active Geometry foldPAM

The previous section has shown that a range of force-strain relationships can be realized by actuators fabricated to have different fold ratios. While this indicates that we can pre-program the behavior of an actuator with folding, we can also control an actuator by actively varying its fold ratio. This capability may be interpreted in two ways: (1) as a method for tuning the stiffness of the actuator for a given pressure; and (2) as a way to control the motion of the actuator by changing the geometry. In this section we implement a tunable fold ratio device and use the device to regulate its length at a desired position with feedback control when an external load is applied.

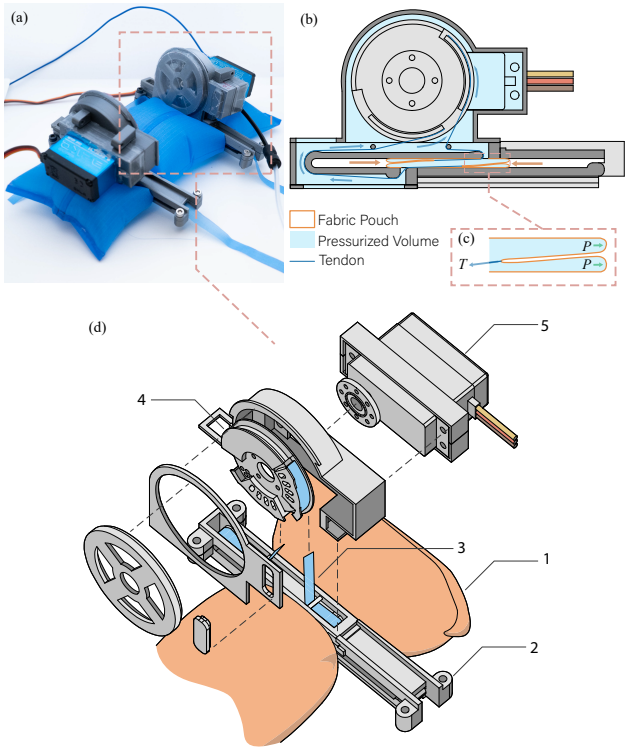

Fig. 8. Composition of the Active foldPAM device. (a): a photo of the prototype; (b): a section view of the rigid frame at one end, showing the transmission mechanism; (c): Enlarged view of the fabric pouch showing the antagonistic pressure force P and the tension force T in the tendon; (d): Exploded view of the rigid frame assembly on one end(1: Fabric Pouch; 2: Rigid Constriction; 3: Tendon; 4: Driving Wheel; 5: Servo Motor).

A. Design and Fabrication

As shown in Figure 8, the device consists of a fabric pouch attached to a pair of rigid frames. The frame constricts the ends of the actuator to have a thin geometry as in the static foldPAM units and also allows actuation of the fold-ratio adjustment. The portion of the pouch bounded by the rigid frames produces the strain of the actuator; while the portions extended beyond the frames does not contribute to the contraction, they make deformation of the pouch easier.

To realize a change in fold ratio, we need to enable linear motion of the points at the end of each edge of the actuator. This is enabled by an antagonistic, tendon-driven mechanism embedded in the rigid frames, as illustrated in Figure 8(b), (c). At each end of the actuator, a pair of active tendons is connected to the inside of the fabric pouch and routed through a channel in the rigid frame, with their other end attached to a wheel driven by a servo motor. The channel and the housing for the servo motor is sealed to retain pressure in the actuator, creating the pressurized volume shown shaded in Figure 8(b). The edges of the fabric pouch are pulled inwards at equal rate when the wheel rotates counter-clockwise, increasing the fold ratio f_r for the unit. When the wheel rotates clockwise, it releases the tendon, and the interior pressure in the fabric pouch causes it to expand laterally, thereby reducing the f_r.

In our implementation, the fabric pouch is fabricated with identical rip-stop nylon fabrics and silicone adhesive as the static-geometry units. The structural components of the rigid frame are 3D-printed with PLA material by a FDM process. A thin layer of solvent-based, gap-filling adhesive (TAMIYA Inc., Shizuoka, Japan) is applied to the interior surface of all pressurized chambers to ensure a seal. A servo motor (FT5330M, Feetech, Guangdong, China) operating at 7.4V is installed on each of the rigid frames to actuate the wheels.

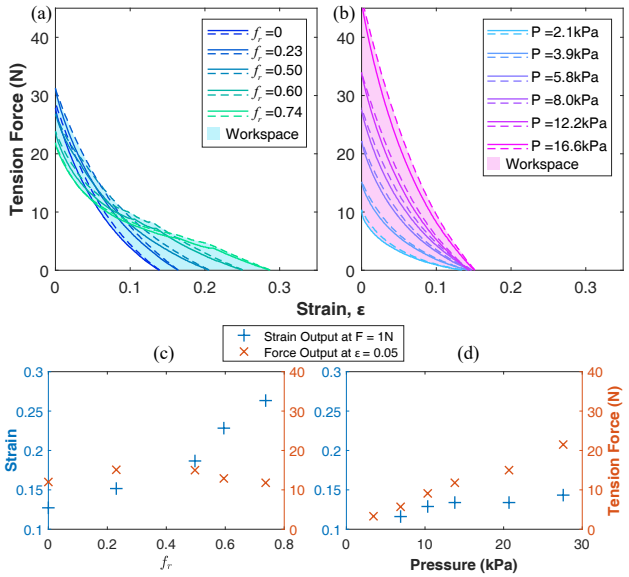

Fig. 9. The force-strain relation of the Active foldPAM device, when (a) the internal pressure is kept at 8.0kPa and f_r is varied between 0 and 0.74 and (b) under a constant $f_r = 0$ and the pressure changes varies from 2.1kPa to 16.6kPa. The area bounded by the force strain curves give the workspace of the Active foldPAM device.

B. Experimental Validation

1) Force-Strain Characterization: The experiment is performed with the same testing apparatus as in Section III-C, except that the fixtures on the test stand and the force gauge are modified to install the Active foldPAM prototype. To compare the effects of actively controlling the geometry and the internal pressure of the device, we perform two sets of experiments, where the fold ratio f_r varies from 0 to 0.74 at a constant pressure of 8.0kPa for the first experiment, and the internal pressure varies from 2.1kPa to 16.6kPa at a constant f_r of 0 for the second. The upper bound of the tested values are the maximum folding and pressure that the prototype can sustain. Notably, the maximum measured f_r exceeds the theoretical limit of the fold ratio at 0.67 due to material elasticity. The result of the experiment is shown in Figure 9.

While one can observe changes in both maximum strain and maximum tension as the fold ratio is varied (Figure 9 (c)), only the maximum force shows monotonic change when the pressure is varied (Figure 9 (d)), which is consistent with the previous literature [20]. Except when f_r is small, increasing f_r results in decreased maximum force and increased strain (i.e., changing the fold ratio "trades" tension for strain, or vice versa). Similar to the previously used "design space" for static foldPAM units, we define a "workspace" for the

Active foldPAM, which is the area bounded by all the curves on the force-strain plane and hence contains all the combinations of force and strain attainable for the device by varying the control input.

The workspace shows distinct area distribution under the two control inputs tested: for the geometric control, the workspace covers a relatively large area at low force, whereas pressure control allows little adjustment at such force output as the force-strain curve converges to a single point. On the other hand, while the workspace under pressure control spans a large range of forces at low strain, the workspace for geometric control shrinks significantly at such strain and displays a non-linear fold-to-force mapping. For example, consider two cases of constant output: in Figure 9(c), with geometric control, the device allows its strain to vary across a range of approximately 0.3 while giving a constant 1N force output, while pressure control in Figure 9(d) only yields a range of 0.15; however, pressure control allows a larger range of force output under a constant ε of 0.05, as compared to the geometric control that effectively cannot tune the force.

2) Open-Loop, Fold-Ratio-to-Output Characterization: As shown in Figure 10(d), the prototype is mounted vertically with the lower end sliding freely in a guiding slot, which constrains the motion to be one-dimensional. The setup is placed in the view of a motion capture system (Impulse X2E, PhaseSpace Inc., CA) and three position tracking markers are placed on the rigid frame at the lower end. The Active foldPAM is initially at zero folding with the driving motor set to 0° and, at $t = 0s$, the servo motors mounted on both ends begin rotating to a set point of 160°, resulting in a maximum w_f of 67mm. The device pressure is 8.0kPa, controlled by a pressure control valve (QB3, Proportion Air, McCordsville, IN), and it is only subjected to its own weight, which is approximately 100 grams. Both the servo and the pressure control valve are interfaced to a computer with an Arduino Mega 2560 microcontroller, which also transmits angle feedback in real-time. The value of w_f is estimated from the servo angle feedback with a fitted polynomial.

The recorded servo angle and position output of the experiment are presented in Figure 10(a), (b), and the motion sequence of the prototype is shown in Figure 10(c). While the servo motor starts to rotate at $t = 0s$, the motion of the device starts at approximately 0.2s, indicating a backlash due to the fabric pouch and tendon elasticity. A total travel (Δz) of 14mm is observed. The value of w_f and Δz in Figure 10 is normalized with respect to W_0 and l_0 respectively, giving the relation between fold ratio f_r to change in strain $\Delta\varepsilon$ in Figure 10(b), which appears to be highly linear.

C. Closed Loop Control through Geometry Change

Finally, we demonstrate that an Active foldPAM device can realize closed-loop control of position output. In particular, we suppose a scenario in which a step change load of 150g mass (1.47N under gravity) is applied to the initially unloaded foldPAM and the device attempts to restore its position by adjusting the fold ratio, while keeping a constant internal pressure of 3.9kPa. As a comparison, a separate

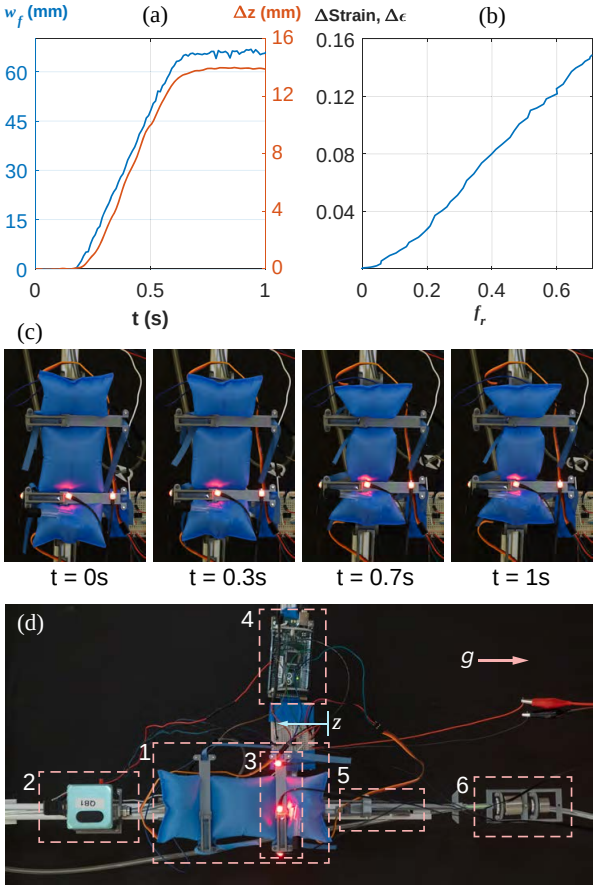

Fig. 10. (a): open-loop response of a vertically placed Active foldPAM device, when the device is commanded to travel from 0 fold to the maximum folding possible. The plot shows the folded length w_f estimated from servo angle feedback and the displacement at the lower end of the device. (b): The relation between fold ratio and the change in strain obtained from the result in (a). (c): The Active foldPAM during the experiment, from $t = 0s$ to $t = 1s$. (d): The experiment set up used in Section IV-B.2 and IV-C, with the downward direction indicated by g (1: The Active foldPAM prototype; 2: pressure control valve; 3: motion capture marker; 4: microcontroller; 5: guiding rail; 6: external load).

experiment is carried out at a constant fold ratio of 0 while the pressure is tuned to compensate for the displacement due to the applied load. The pressure supply is commanded to vary between 6.9kPa and 27.6kPa, and the pouch achieves a lower pressure range of 3.9kPa to 16.7kPa due to leaks in the prototype. The same set up for the open-loop displacement characterization is used in this demonstration. The real-time position feedback from the motion capture system is used to compute the error value, and a proportional-integral (PI) controller is used to generate the control signal for the servo motor and the pressure regulator for the two experiments respectively. The control loop runs at a frequency of 6 Hz.

Figure 11 gives the result from the experiments. The two experiments see an average initial error of 5.8mm. Due to the characteristics of the controller, in Figure 11(a) the control signal for the servo motor gradually increase , whereas the pressure control value in Figure 11(b) jumps instantaneously to the saturating level. However, the geometric control results in near-zero steady-state error, while a 1.5mm steady-state

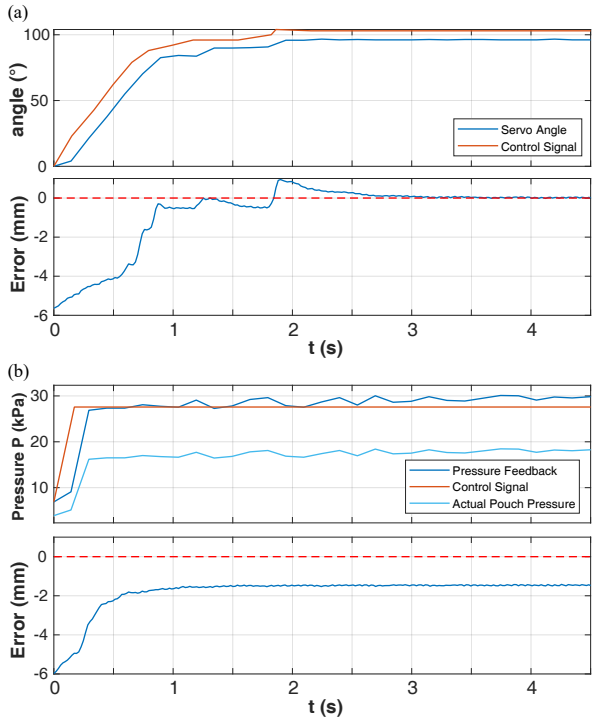

Fig. 11. A PI control loop is implemented for the Active foldPAM device to regulate its position output when a step change in load of approximately 150 grams is applied. The figure shows the response of (a) geometry-based control and (b) pressure-based control. For (b) both the pressure feedback value from the supply and the actual pressure in the prototype is shown.

error is observed for pressure control. This reflects the observation in Section IV-B.1, that the geometric actuation results in a larger strain workspace at a small, constant load, while the ability of the pressure to compensate for strain errors is limited. It should be acknowledged, however, that the performance of pressure control is limited by the prototype's ability to hold sufficiently high pressure. The difference in workspace shape additionally suggests that actuators with both pressure and geometry actuation for closed-loop control can better respond to a wide range of force inputs.

V. Conclusion and Future Work

In this paper, we presented a new design of a pneumatic actuator for which the force and strain can be tuned by varying the end geometry, namely the width of the laterally folded portion. This feature can be used for both pre-programming and actively controlling an actuator unit. With this principle, we explored the concept of "geometric control", as opposed to the traditional pressure-based control strategy, and showed that it responds linearly to the control input and enables a different workspace than pressure control alone.

Future work on foldPAMs will focus on modeling the actuator behavior, for which approximations by existing models gives limited accuracy. For Active foldPAM units, the actuation of the geometry is currently bulky so a compact, lightweight source of actuation is needed to implement geometric change at a form factor that is favorable for applications. Finally, the concept of geometric control raises a wide range of new questions to explore, such as its applicability to other types of pneumatic actuators, and the potential of achieving programmable actuator trajectory with passive geometry-changing mechanisms.

References

[1] H. A. Baldwin, "Realizable models of muscle function," in *Biomechanics*, D. Bootzin and H. C. Muffley, Eds. New York, NY: Springer US, 1969, pp. 139–147.

[2] D. Rus and M. T. Tolley, "Design, fabrication and control of soft robots," pp. 467–475, 5 2015.

[3] M. Zhu, A. H. Memar, A. Gupta, M. Samad, P. Agarwal, Y. Visell, S. J. Keller, and N. Colonnese, "PneuSleeve: In-fabric multimodal actuation and sensing in a soft, compact, and expressive haptic sleeve." Association for Computing Machinery, 4 2020.

[4] G. Andrikopoulos, G. Nikolakopoulos, and S. Manesis, "A survey on applications of pneumatic artificial muscles," 2011, pp. 1439–1446.

[5] E. W. Hawkes, D. L. Christensen, and A. M. Okamura, "Design and implementation of a 300% strain soft artificial muscle," vol. 2016-June. Institute of Electrical and Electronics Engineers Inc., 6 2016, pp. 4022–4029.

[6] S. Li, D. M. Vogt, D. Rus, and R. J. Wood, "Fluid-driven origami-inspired artificial muscles," *Proceedings of the National Academy of Sciences*, vol. 114, no. 50, pp. 13 132–13 137, 2017. [Online]. Available: https://www.pnas.org/doi/abs/10.1073/pnas.1713450114

[7] C. Tawk, M. in het Panhuis, G. M. Spinks, and G. Alici, "Bioinspired 3D printable soft vacuum actuators for locomotion robots, grippers and artificial muscles," *Soft Robotics*, vol. 5, no. 6, pp. 685–694, 2018, pMID: 30040042. [Online]. Available: https://doi.org/10.1089/soro.2018.0021

[8] F. Daerden and D. Lefeber, "The concept and design of pleated pneumatic artificial muscles," *International Journal of Fluid Power*, vol. 2, pp. 41–50, 2001.

[9] N. D. Naclerio and E. W. Hawkes, "Simple, low-hysteresis, foldable, fabric pneumatic artificial muscle," *IEEE Robotics and Automation Letters*, vol. 5, pp. 3406–3413, 4 2020.

[10] F. Ilievski, A. D. Mazzeo, R. F. Shepherd, X. Chen, and G. M. Whitesides, "Soft robotics for chemists," *Angewandte Chemie - International Edition*, vol. 50, pp. 1890–1895, 2 2011.

[11] J. Ou, M. Skouras, N. Vlavianos, F. Heibeck, C. Y. Cheng, J. Peters, and H. Ishii, "AeroMorph - heat-sealing inflatable shape-change materials for interaction design." Association for Computing Machinery, Inc, 10 2016, pp. 121–132.

[12] J. D. Greer, T. K. Morimoto, A. M. Okamura, and E. W. Hawkes, "Series pneumatic artificial muscles (sPAMs) and application to a soft continuum robot." Institute of Electrical and Electronics Engineers Inc., 7 2017, pp. 5503–5510.

[13] R. S. Diteesawat, T. Helps, M. Taghavi, and J. Rossiter, "Characteristic analysis and design optimization of bubble artificial muscles," *Soft Robotics*, vol. 8, pp. 186–199, 4 2021.

[14] N. Kellaris, V. G. Venkata, G. M. Smith, S. K. Mitchell, and C. Keplinger, "Peano-HASEL actuators: Muscle-mimetic, electrohydraulic transducers that linearly contract on activation," p. 3276, 2018. [Online]. Available: https://www.science.org

[15] F. Connolly, C. J. Walsh, and K. Bertoldi, "Automatic design of fiber-reinforced soft actuators for trajectory matching," *Proceedings of the National Academy of Sciences of the United States of America*, vol. 114, pp. 51–56, 1 2017.

[16] Y. Luo, K. Wu, A. Spielberg, M. Foshey, D. Rus, T. Palacios, and W. Matusik, "Digital fabrication of pneumatic actuators with integrated sensing by machine knitting." Association for Computing Machinery (ACM), 4 2022, pp. 1–13.

[17] Z. Kan, C. Pang, Y. Zhang, Y. Yang, and M. Y. Wang, "Soft actuator with programmable design: Modeling, prototyping, and applications," *Soft Robotics*, 1 2022.

[18] K. T. Yoshida, X. Ren, L. H. Blumenschein, A. M. Okamura, and M. Luo, "AFREEs: Active fiber reinforced elastomeric enclosures; afrees: Active fiber reinforced elastomeric enclosures," 2020.

[19] A. J. Veale, S. Q. Xie, and I. A. Anderson, "Characterizing the Peano fluidic muscle and the effects of its geometry properties on its behavior," *Smart Materials and Structures*, vol. 25, 5 2016.

[20] R. Niiyama, X. Sun, C. Sung, B. An, D. Rus, and S. Kim, "Pouch motors: Printable soft actuators integrated with computational design," *Soft Robotics*, vol. 2, pp. 59–70, 6 2015.